Proceedings of the Combustion Institute 41 (2025) 105885

Contents lists available at ScienceDirect

Proceedings of the Combustion Institute

journal homepage: www.elsevier.com/locate/proci

Laminar and turbulent hydrogen-enriched methane flames: Interaction of thermodiffusive instabilities and local fuel demixing

Hendrik Nicolai [a,*], Vinzenz Schuh [a], Antonia Bähr [a], Max Schneider [a], Felix Rong [a], Driss Kaddar [a], Mathis Bode [b], Christian Hasse [a]

[a] Technical University of Darmstadt, Department of Mechanical Engineering, Simulation of reactive Thermo-Fluid Systems, Otto-Berndt-Straße 2, 64287 Darmstadt, Germany

[b] Jülich Supercomputing Centre, Forschungszentrum Jülich GmbH, Jülich, 52425, Germany

ARTICLE INFO

Keywords:
CH_4/H_2 blends
Thermodiffusive instabilities
Turbulent flames
Direct numerical simulation

ABSTRACT

Blending hydrogen with methane provides a practical approach for transitioning existing energy infrastructure to hydrogen-based carriers. However, under fuel-lean conditions, increasing the hydrogen content causes flames to transition rapidly from methane-like combustion to hydrogen-dominated flames, primarily driven by thermodiffusive instabilities that significantly enhance turbulent flame speeds. This study systematically examines lean methane/hydrogen/air flames of varying complexity, from three-dimensional laminar unstable cases to turbulent jet flames at two different Reynolds numbers, with an emphasis on the impact of the distinct molecular transport properties of hydrogen and methane. The large-scale simulations reveal that these blends exhibit instabilities even under turbulent conditions, albeit to a lesser degree than pure hydrogen flames. Nonetheless, synergistic interactions between turbulence and thermodiffusive instabilities lead to notable increases in turbulent flame speed and reactivity factors (I_0) at higher Reynolds/Karlovitz numbers. Moreover, beyond the effects of overall non-unity Lewis number, the different diffusivity of hydrogen and methane (i.e., non-equal Lewis numbers) significantly influence the formation and intensity of intrinsic flame instabilities. These findings underscore the importance of thermodiffusive instabilities in methane/hydrogen combustion and highlight the need for advanced modeling approaches capable of capturing local demixing effects under turbulent flows conditions.

1. Introduction

To facilitate the transition of existing energy infrastructure to hydrogen as an energy carrier, short- and mid-term approaches emphasize blending hydrogen with natural gas (primarily methane) at progressively higher hydrogen contents. Under fuel-lean conditions, this shift in composition triggers a rapid change in combustion properties, transitioning from methane-like behavior to hydrogen-dominated flames with notably higher turbulent flame speeds, driven largely by intrinsic thermodiffusive instabilities [1].

These instabilities originate from the imbalance between mass and thermal diffusion, creating regions along the flame front that burn at varying intensities, with some areas exhibiting enhanced combustion while others burn less intensely. In hydrogen flames, the low Lewis number amplifies small perturbations, resulting in highly wrinkled flame fronts, increased flame speed, and pronounced variations in reaction rates. Despite extensive theoretical analyses [2,3], analytical modeling remains challenging, necessitating the use of large-scale simulations to investigate laminar instabilities.

In turbulent flows, intrinsic instabilities play a significant role at low Karlovitz numbers, whereas at higher Karlovitz numbers, turbulence tends to dominate, suppressing molecular effects. Yet, the exact region of influence remains unclear. Experimental and numerical studies in form of Direct Numerical Simulation (DNS) studies confirm super-adiabatic temperatures and flame distortion from thermodiffusive instabilities [1,4], with Aspden et al. [5] showing a strong enhancement of reaction rates in lean hydrogen flames at low Karlovitz numbers. As turbulence increases, cellular structures distort, heat release and fuel consumption decorrelate, and equivalence ratio fluctuations diminish—though differential diffusion persists even at large Karlovitz numbers [5–7].

Berger et al. [8] demonstrated that thermodiffusive instabilities are amplified in turbulence, increasing flame curvature and strain rates, resulting in turbulent flame speeds up to 15 times the laminar burning velocity. A follow-up DNS study [9] on lean hydrogen/air slot-burner flames at Karlovitz numbers $Ka = 10, 50, 230$ and a constant jet

* Corresponding author.
E-mail address: nicolai@stfs.tu-darmstadt.de (H. Nicolai).

https://doi.org/10.1016/j.proci.2025.105885
Received 2 May 2025; Accepted 21 September 2025
Available online 10 October 2025

Reynolds number reported super-adiabatic temperatures, high turbulent flame speeds, and finger-like flame structures at low Ka. At higher Karlovitz numbers, turbulence prevailed, boosting the stretch/reactivity factor I_0 via rising mean strain rates, while mixture fraction fluctuations peaked at intermediate Ka, influencing local reactivity and flame response.

Although the previous studies predominantly focused on pure hydrogen flames, there has been growing interest in fuel blends. Also, in ammonia/hydrogen (NH_3/H_2) blends, the fuel composition and equivalence ratio crucially affect consumption rate enhancement, driven by the preferential diffusion of light species, which locally enriches the flame front and intensifies thermodiffusive effects, especially in lean conditions. For example, in turbulent NH_3/H_2 flames, the need to account for thermodiffusive instabilities is recognized [10], yet the limited range of investigated compositions [11–13] raises questions about how far and how strongly these effects influence turbulent NH_3/H_2 flames under varying conditions. Meanwhile, flames with similar flame speeds exhibit comparable strain rates, and flame curvature systematically declines with increasing equivalence ratio and H_2 content in NH_3/H_2 mixtures.

In contrast, methane/hydrogen (CH_4/H_2) blends have received significantly less attention, leaving a key knowledge gap regarding their behavior under different operating conditions. While both early and more recent experimental studies have examined the impact of hydrogen addition to methane flames [14–16], the majority of these investigations focus on near-stoichiometric conditions, where thermodiffusive instabilities are not prominent. The few existing studies that include thermodiffusive effects focus on laminar flames in simplified configurations [17–19]. Although recent studies [20,21] suggest additional complexities in the interaction of CH_4/H_2 blends with these instabilities, a comprehensive understanding remains elusive. An early investigation by Hawkes et al. [22] employed two-dimensional DNS with a reduced chemical mechanism to compare lean premixed CH_4/H_2 flames, with and without hydrogen enrichment, focusing on flame stability and pollutant formation. Their results showed that hydrogen addition increases flame speed, surface area, and burning rate, primarily due to preferential diffusion and enhanced resistance to quenching, while reducing CO emissions and increasing NOx formation. In this work, we extend previous studies by examining thermodiffusive instabilities in CH_4/H_2 flames under both laminar and turbulent conditions, with a focus on their impact on flame dynamics and implications for model development. The specific objectives of this study are:

1. Investigate thermodiffusive instability (TDI) development in both laminar and turbulent CH_4/H_2 flames under identical conditions to assess regime-dependent effects.
2. Identify and quantify the synergistic interaction between turbulence and TDI, linking instability growth to reactivity changes and flame front dynamics.
3. Examine preferential diffusion between CH_4 and H_2 (fuel demixing) and its independent role in instability formation.
4. Derive insights to guide the development of predictive models that capture TDI and preferential diffusion effects in fuel blends.

2. Configuration and numerical setup

Large-scale three-dimensional DNS are conducted for three lean premixed CH_4/H_2/air flames: one laminar case in a periodic rectangular box and two turbulent flames in a jet burner configuration with a surrounding coflow of exhaust gas. All simulations use a fuel mixture of 80 vol.-% H_2 and 20 vol.-% CH_4, with an equivalence ratio of $\phi = 0.6$, an unburnt gas temperature of $T_u = 300$ K, and a pressure of $p = 1$ atm.

To compare the tendency of the mixture to become TD unstable, the growth rate ω_2 is computed and compared against pure H_2 mixtures commonly found in the literature. For details on the methodology, the interested reader is referred to Howarth et al. [23]. While the hydrogen molar fraction offers a useful estimate for comparing instability

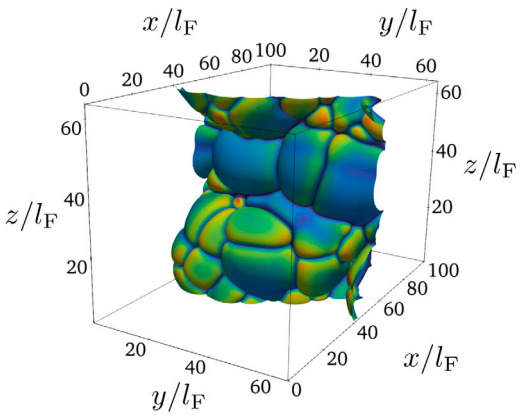

Fig. 1. Snapshot of the flame surface area of the laminar case colored by the heat release. The flame surface area is defined by an iso-surface of the temperature of 1000 K. The initially flat flame is stabilized in the center of the domain by regulating the inlet velocity.

tendencies between pure H_2 and CH_4/H_2 mixtures, such comparisons are inherently non-trivial under fixed global conditions. Variations in effective Lewis numbers and the reduced hydrogen content across the flame front in blends can shift the flame closer to the unstable regime, even at more stabilizing global equivalence ratios. Moreover, matching mixtures solely based on hydrogen content may yield significantly different global ϕ values and altered TDI behavior. To support a more detailed interpretation, we provide the full results of numerically obtained dispersion relations in the Supplementary Material.

For the CH_4/H_2 blend ($X_{H_2} = 0.8$, $\phi = 0.6$, $T = 300$ K, $p = 1$ atm), a positive growth rate of $\omega_2 = 1.625$ is obtained. In contrast, pure H_2 flames studied in literature shows markedly higher instability levels, with $\omega_2 = 2.895$ at $\phi = 0.5$ [4] and $\omega_2 = 7.142$ at $\phi = 0.4$ [8], highlighting the significantly lower instability of the blend and prompting questions about its relevance in both laminar and turbulent regimes.

The three-dimensional DNS of the laminar, initially planar CH_4/H_2/air flame serves as a baseline case for comparison. This setup enables a rigorous separation of turbulence effects from intrinsic flame instabilities in the flame evolution. As shown in Fig. 1, the unburned mixture enters at the lower x-boundary, while burned gas exits at the upper x-boundary, with periodic boundary conditions applied in the lateral (y- and z-) directions. The domain spans $L_x = 100\,l_F$ in lateral direction and has a cross section of $L_y = L_z = 64\,l_F$, which confines large-scale corrugations, preventing a domain-independent consumption speed, but still captures local flame dynamics and fuel demixing (i.e., I_0 is expected to be independent of the domainsize), which are primarily governed by small-scale wrinkling [8,24]. The simulation is initialized with a harmonically perturbed flat flame, and the inlet velocity is adjusted to keep the flame stabilized in the domain. Similar to pure H_2 flames, Fig. 1 reveals strong heat-release variations due to thermodiffusive instabilities, leading to the formation of cellular structures and distinct cusps, resulting in a highly corrugated flame front.

For the two turbulent flames, the configuration illustrated in Fig. 2, consists of a turbulent jet of fresh gases surrounded by a pilot containing burned products of the corresponding jet mixture, with a temperature equal to the adiabatic flame temperature of $T_b = 1760$ K. The jet has a radius of $R_{\text{Jet}} = 4.5$ mm and is separated from the pilot by an adiabatic wall with no-slip velocity conditions. The domain is sufficiently large to prevent any interference from the outlet or lateral boundaries with the flame. A steady, laminar coflow is imposed at the pilot with a constant, non-fluctuating velocity of 15% of the jet's bulk velocity u_{bulk}.

Between the two cases, the inlet velocity is varied which results in Reynolds numbers of $Re = 6000$ and $Re = 12\,000$, respectively. The inlet

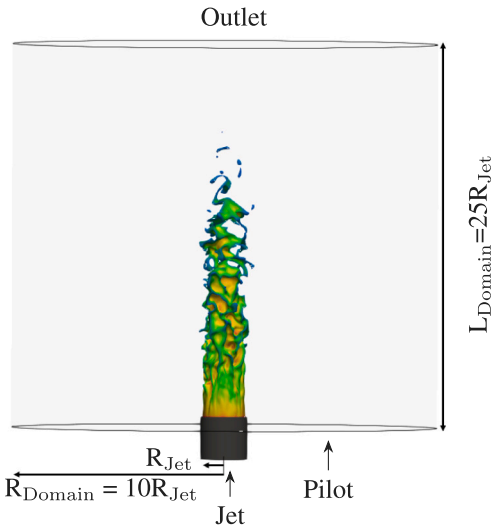

Fig. 2. Visualization of the turbulent jet flame represented by an isosurface of temperature that is colored by the heat release.

Table 1
Simulation parameters and features of the two turbulent flames with 80 Vol.-% H_2 in CH_4.

	Intermediate turbulence	Low turbulence
D (mm)	4.5	4.5
U (m/s)	25	12.5
U_{co} (m/s)	3.75	1.875
s_l (cm/s)	34.73	34.73
l_f (μm)	500	500
l_f/Δ	12	12
Re	12 000	6000
Ka	60	20
N_{Grid}	$923{\cdot}10^6$	$690{\cdot}10^6$

velocities of the central jet are mapped on-the-fly using overset meshes from an auxiliary fully developed turbulent pipe flow DNS. To ensure fully developed turbulence in the jet, the auxiliary pipe is extended to $16R$, and velocity recycling is applied in the auxiliary pipe. An overview of the simulation parameters is provided in Table 1.

2.1. Numerical methods and models

For the large scale simulation conducted here, two distinct solvers tailored to respective numerical challenges of each setup are used: For the laminar case, the adaptive mesh refinement (AMR) code PeleLMeX [25] and for the turbulent cases the spectral-element solver nekCRF [26]. Both solvers assume ideal gas and employ the low Mach number assumption [27] for the reactive Navier–Stokes equations using the Hirschfelder–Curtiss approximation for scalar diffusion velocity [28]. A correction velocity for the species diffusion is employed to ensure mass conservation. The fluid is assumed to be an ideal gas and chemical reactions are modeled by the reduced mechanism of Smooke et al. [29] that contains 16 species and 25 reactions.

In the simulation performed with PeleLMeX, the governing equations are discretized in space and time using second-order schemes [25]. Following the approach of Howarth et al. [23], the simulation employs three levels of adaptive mesh refinement based on a threshold criterion: a buffer of three fine cells is added around regions where the HO_2 mass fraction exceeds 30% of its 1D peak value. Starting from a base grid of 400 × 256 × 256, this strategy yields an effective resolution of 3200 × 2048 × 2048.

The turbulent DNS are performed using the spectral element method code nekRS [30], coupled with the chemistry plugin nekCRF [26]. NekRS employs high-order spectral elements, where the solution, data, and test functions are represented as locally structured Nth-order tensor product polynomials on a globally unstructured set of E conforming hexahedral brick elements. Time integration follows a semi-implicit splitting scheme [27], where the time derivative is approximated using a kth-order (up to $k = 3$) backward differentiation formula (BDFk), resulting in an implicit treatment of viscous and pressure terms. Advection and forcing terms are handled via kth-order extrapolation (EXTk). The present study employs a 7th-order spatial discretization and a 3rd-order temporal discretization. The thermochemical subsystem is integrated without further splitting of diffusion and reaction terms using CVODE.

3. Results and discussion

3.1. Analysis of laminar TDI

Fig. 3 presents a slice through the three-dimensional flame front of the laminar case, with all quantities normalized by the peak value of a freely-propagating flame. As expected, key characteristics of thermodiffusive unstable flames persist as seen in lean hydrogen/air mixtures. The normalized temperature field exhibits super-adiabatic regions, where local temperatures exceed the nominal adiabatic flame temperature of the inlet mixture, particularly in positively curved regions. Compared to previous studies on lean hydrogen flames [1], the temperature rise occurs more gradually, which can be attributed to the slightly richer equivalence ratio of $\phi = 0.6$, leading to an overall increase in the effective Lewis number. As seen in both the normalized Bilger mixture fraction Z_{Bilger} and the normalized H_2O mass fraction, these temperature increases are driven by strong fuel diffusion into positively curved regions. This localized fuel enrichment enhances reactivity, as indicated by the elevated normalized OH mass fraction.

3.2. Turbulent CH_4/H_2/air jet flames

Fig. 4 presents the normalized temperature, normalized Bilger mixture fraction, the normalized H_2O mass fraction, and the normalized OH mass fraction for both Reynolds numbers of the turbulent jet flame. As before, normalization is based on the peak values from one-dimensional flame simulations..

Examining the normalized temperature contours, regions with temperatures exceeding the adiabatic flame temperature are clearly visible. These arise primarily from the high-strain region above the pipe walls, which encloses the inner reaction layer. Additionally, localized temperature hot spots appear in areas of high flame curvature. By correlating this observation with the local mixture fraction contour, the formation of these pockets can be attributed to thermodiffusive effects, driven by the non-unity Lewis number of H_2. Similarly, the normalized Y_{H_2O} mass fraction exhibits local maxima in these strongly curved regions, underlining that local transport effects due to differential diffusion lead to super-adiabatic states. That these states affect the flame can be seen in the $Y_{OH,n}$ contour, which clearly demonstrates high local $Y_{OH,n}$ values in these regions, suggesting enhanced reactivity.

Comparing the two simulations clearly shows how the increased Reynolds and Karlovitz numbers affect the flame. Doubling the Reynolds number by raising the inlet velocity extends the high-Re flame further downstream, while intensified local velocity fluctuations create a more corrugated flame front and thus a larger flame surface area. In both cases, two regions exceed the adiabatic flame temperature: as before, the outer high-strain zone elevates temperatures, but the high-Re flame additionally develops numerous small pockets with locally super-adiabatic states. This increase in smaller hot spots arises from greater local curvature along the more corrugated flame front. Despite these differences, the absolute values of both super-adiabatic temperatures and local mixture fraction remain similar for the low- and high-Re flames.

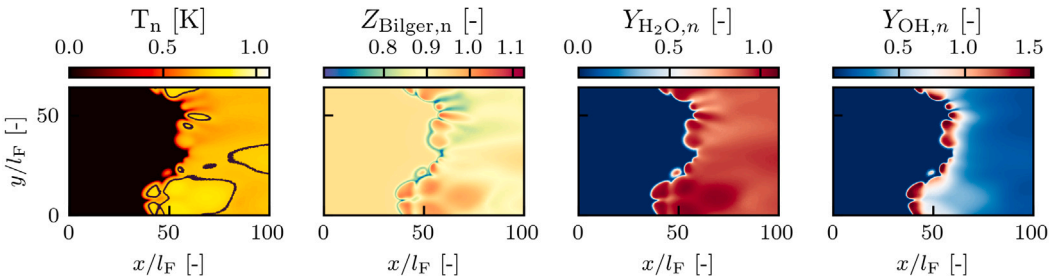

Fig. 3. Instantaneous snapshots of the normalized temperature T_n, Bilger mixture fraction $Z_{Bilger,n}$, $Y_{H_2O,n}$ mass fraction and $Y_{OH,n}$ mass fraction on a slice through the laminar flame. The temperature contour features a temperature isoline at the adiabatic flame temperature to highlight regions of super-adiabatic temperatures.

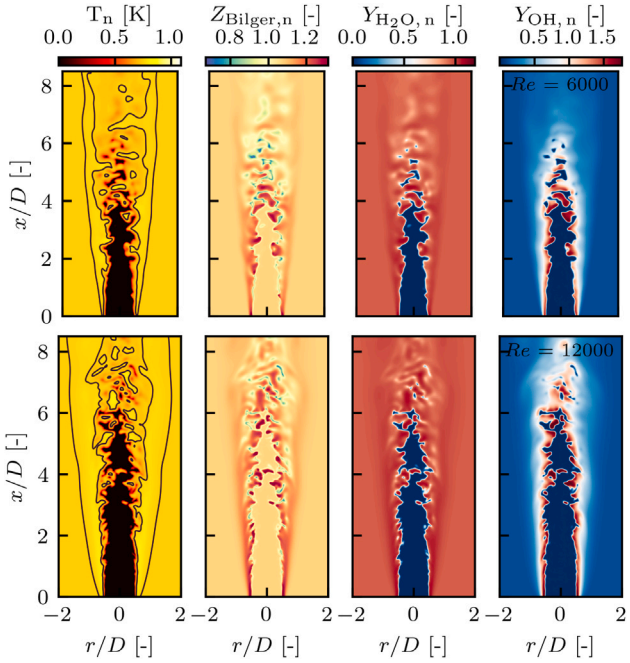

Fig. 4. Instantaneous snapshots of the normalized temperature T_n, Bilger mixture fraction $Z_{Bilger,n}$, $Y_{H_2O,n}$ mass fraction and $Y_{OH,n}$ mass fraction for the two turbulent flames (Re = 6000 top row; Re = 12 000 bottom row). The normalized temperature contour features a temperature isoline at the adiabatic flame temperature to highlight regions of super-adiabatic temperatures.

3.3. Analysis of the reactivity factor I_0

In the following analyses, only the flame above the height of $x/D \geq 3.5$ is considered for the jet flames, since near the burner rim high-strain values dominate the flame propagation rather then thermodiffusive instabilities. To quantify these observations, the local flame characteristics are analyzed using at least 10 000 pathlines for each flame, which traces the gradient of the reaction progress variable PV, corresponding to local trajectories of one-dimensional flame structures. This approach follows the methodology of Howarth and Aspden [31], who defined tubes crossing the flame front to examine local flame properties.

Fig. 5 presents the reactivity factor I_0, the normalized flame thickness l_f/l_f^0, and the normalized consumption speed $s_c/s_{l,ref.}$ for the laminar freely propagating flame and turbulent jet flames.

The reactivity factor I_0, also referred to as stretch factor or burning efficiency, is defined as $I_0 = (s_c/s_{l,ref.})/(A/A_l)$, with the normalized consumption speed and the flame surface area increase A/A_l. For the current approach using flame trajectory pathlines, the reactivity factor is the mean value of the normalized consumption speed over all pathlines: $I_0 = \langle s_c/s_{l,ref.} \rangle_{pathlines}$, shown by the black dashed line in Fig. 5, similar to [31].

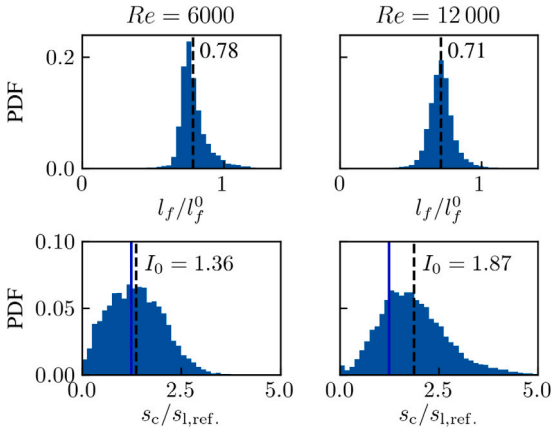

Fig. 5. PDFs of the local thermal flame thickness and the reactivity factor I_0 of the turbulent jet flames. The blue line denotes the reactivity factor of the laminar reference three-dimensional unstable flame with I_0^{lam} = 1.23.

The results in Fig. 5 indicate that thermodiffusive instabilities are amplified in turbulent flames due to synergistic interactions, as reported by Berger et al. [8]. This is particularly evident when compared to the reference value from the three-dimensional laminar unstable flame, shown in blue in Fig. 5. Specifically, the reactivity factor I_0 increases with higher turbulence levels for low and intermediate Karlovitz numbers, transferring the findings from Berger et al. [9] also for weakly thermodiffusively unstable CH_4/H_2 blended flames.

3.4. Composition space

Next, the behavior of the two fuels over the flame front across the three simulations is examined. To this end, the fuel mass fractions of Y_{H_2} and Y_{CH_4} are plotted as a function of temperature T in Fig. 6. In addition to the black lines, which represent the conditional average for each of the three simulations, a reference laminar unstretched flame is shown in red. This flamelet is computed using Cantera [32] with mixture-averaged transport and the same reaction mechanism as employed in the DNS simulations. The conditional mean from all three simulations closely aligns with the mixture-averaged flamelet, with only minor deviations. A slight underprediction is observed in the laminar case at low temperatures, while for increased turbulence levels, the flamelet exhibits a slight overprediction in the same temperature range. Notably, the Y_{CH_4} mass fraction is well captured by the adiabatic flamelet simulation. However, when considering the scatter of individual data points, distinct differences emerge between the two initially perfectly premixed fuels.

While the CH_4 mass fraction remains nearly constant around the conditional mean across all setups, H_2 exhibits significantly larger scatter. In the laminar case, slightly elevated hydrogen mass fractions are observed. The color of the scatter points indicates that these higher

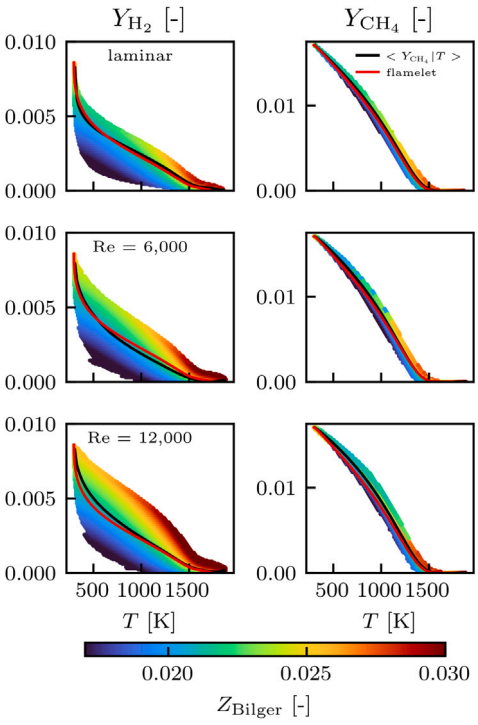

Fig. 6. Composition space of the fuel mass fractions Y_{H_2} (left) and Y_{CH_4} (right) for the three different simulations. Top to bottom: laminar, Re = 6000 and Re = 12 000.

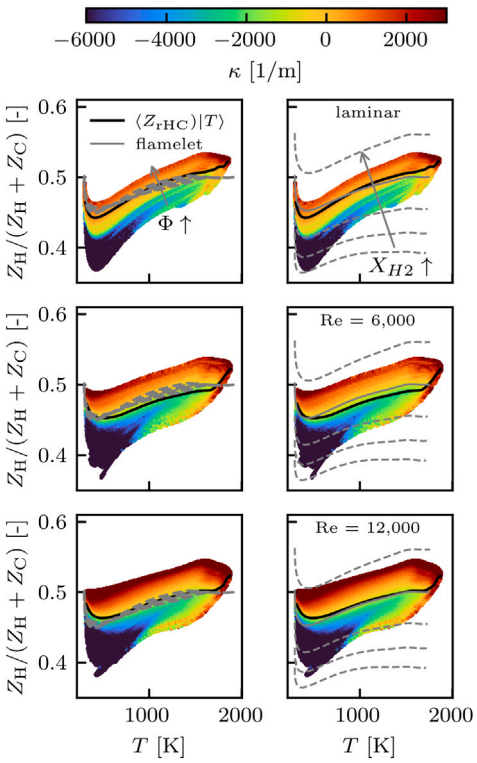

Fig. 7. Composition space of the mixture fraction ratio colored by the local flame curvature for the three different simulations (Top: Laminar; Middle: Re = 6000; Bottom: Re = 12 000). In addition, flamelet variations of equivalence ratio (left) and initial fuel ratios (right) are shown.

H_2 concentrations predominantly occur in regions with high mixture fractions. This suggests that in fuel-rich positively curved regions of the flame front, as highlighted in Fig. 4, H_2 enrichment plays a dominant role in increasing total fuel to air ratio. Conversely, scatter points below the conditional mean are primarily associated with fuel-lean regions. This implies that in negatively curved regions, H_2 diffuses away, leaving the flame propagation largely governed by methane conversion.

Examining the two turbulent cases, similar trends are observed. However, with increasing turbulence intensity, the local mass fraction of H_2 tends to rise. This effect can be attributed to the enhanced strain induced by stronger turbulent fluctuations. A comparable behavior has been reported for pure hydrogen flames by Berger et al. [9].

In the following, the observed preferential diffusion between H_2 and CH_4 is examined more closely. This analysis incorporates the local curvature κ:

$$\kappa = \nabla \cdot \mathbf{n} \quad \text{with} \quad \mathbf{n} = -\nabla C_{H_2O}/|\nabla C_{H_2O}|, \tag{1}$$

as a key metric to characterize the flame geometry to facilitate the correlation of local mixing states with local flame front curvature. To assess demixing at higher temperatures, where both fuels are fully consumed, a mixture fraction-based approach is introduced instead of directly using the fuel species. In a four-element system (C, O, H, N), a complete description requires five controlling variables: the elemental mixture fractions of C, O, and H, along with temperature T. The nitrogen fraction can be inferred from the elemental unity constraint. Since the focus is primarily on the demixing of hydrogen and carbon, a new parameter is introduced to quantify this effect: the ratio of their respective elemental mass fractions.

$$Z_{rHC} = \frac{Z_H}{Z_H + Z_C}. \tag{2}$$

Using the two introduced quantities, curvature and mixture fraction ratio, the results of the three simulations are depicted in Fig. 7. In addition, two different combinations of flamelet variations are shown: On the left, a standard variation of the fuel-air equivalence ratio is shown between $\phi = 0.5 - 0.7$. This parameter, in combination with a reaction progress variable, is commonly employed in flamelet tabulation approaches [20]. On the right, the variation of the H_2-content in the fuel (from 65%-Vol. H_2 to 85%-Vol. H_2) for the same equivalence ratio $\phi = 0.6$ is depicted.

As already deduced from the thermochemical state of the fuel fractions, the mixture fraction ratio shows a significant scatter in the preheat region of the flame. Considering also the values of the curvature, one can clearly correlate this demixing behavior with local flame curvature. Minimum mixture fraction ratio values, indicating lower contents of hydrogen, are always found in the region of strongly negative curvature. In contrast, locations of high ratios, i.e., increased hydrogen contents, are associated with positive curvature.

A comparison of the simulation results with the reference flamelets shows that the conditional mean of the DNS data aligns well with the flamelet predictions across all three cases. However, it is important to note that this conditional mean consistently corresponds to the zero-curvature region within the conditional scatter. Notable deviations from the conditional mean occur at very low temperatures in the preheat zone and in the burnt region, where super-adiabatic states cause discrepancies from the reference flamelet. More striking, however, is the significant scatter in the DNS data, particularly at low and intermediate temperatures, which is even more pronounced compared to the scatter in the fuel mass fractions. In these regions, local demixing leads to substantial variations in the hydrogen-to-carbon ratio, which cannot be captured by a simple ϕ variation in the flamelet model.

This becomes even more apparent when analyzing flamelet variations with different initial fuel ratios, where fluctuations of up to 15 vol.-% H_2 are necessary to encompass all scatter points from the DNS simulation. While these flamelets effectively capture the minimum and maximum elemental ratios in the flame, they fail to account

for the super-adiabatic states at a fixed equivalence ratio. This suggests that accurately representing thermodiffusively unstable CH_4/H_2 flames requires independent variation of both the equivalence ratio and the carbon-to-hydrogen mixture fraction ratio to fully capture the complexity of the system.

Comparing the laminar case with the two turbulent cases reveals that fuel demixing remains significant across the investigated turbulence levels. Only a slight reduction in the minimum values of the mixture fraction ratio is observed. Additionally, at high mixture fraction ratios, a slight increase is noticeable with increasing turbulence intensity. This trend is likely driven by enhanced stretch effects resulting from stronger turbulence-flame interactions, a phenomenon also reported by Berger et al. [9].

4. Conclusion

In this study, three large-scale direct numerical simulations (DNS) of lean methane/hydrogen/air flames are conducted under both laminar and turbulent flow conditions. The selected fuel blend and operating condition promotes the development of thermo-diffusive instabilities, enabling a detailed analysis of their formation in laminar flames and their interaction with turbulence. While unstable, the mixture exhibits lower instability levels, characterized by a reduced growth rate ω_2, compared to pure hydrogen. The main conclusions of this study are as follows:

- Across the investigated flow regimes, the development of instabilities was observed in both laminar and turbulent CH_4/H_2 flames under identical conditions, revealing that lean fuel blends exhibit persistent instability behavior. In the turbulent regime, turbulence enhances the thermodiffusive response, highlighting their coupled impact on flame dynamics.
- The role of preferential diffusion between CH_4 and H_2, referred to as fuel demixing, in the development of thermodiffusive instabilities is highlighted. Unlike prior DNS studies focused on single-fuel mixtures, our results demonstrate that fuel demixing remains a distinct and active mechanism, even in the presence of turbulence. Its effects are not suppressed by turbulence–TDI interactions, indicating that demixing and thermodiffusive instabilities can act concurrently but independently influencing the local flame structure.
- These findings have important implications for modeling: The demixing of initially perfectly mixed fuels plays a crucial role in instability formation and must be explicitly accounted for to ensure predictive accuracy in combustion simulations. A modeling approach based on mixture fraction ratios presents a promising strategy for capturing preferential diffusion effects in fuel blends. This ultimately leads to a two-mixture-fraction framework, with each mixture fraction associated with fuel demixing and thermodiffusive instabilities, respectively.

These findings highlight the importance of TD instabilities in methane/hydrogen combustion and the need for advanced flamelet-based models that account for fuel demixing and TD instabilities simultaneously. Future work will focus on extending manifold formulations to include mixture fraction ratios and validating them under realistic conditions.

Novelty and significance statement

The novelty of this research lies in its systematic, high-fidelity analysis of lean methane/hydrogen/air flames across a wide range of configurations — from three-dimensional laminar flames exhibiting intrinsic instabilities to turbulent jet flames at different Reynolds numbers. A key innovation is the detailed investigation of how the distinct molecular transport properties of hydrogen and methane (i.e., non-equal Lewis numbers) influence flame behavior under both laminar and turbulent conditions. It is significant because it demonstrates that thermodiffusive instabilities persist even in turbulent regimes and are amplified through interactions with turbulence, leading to enhanced flame propagation and reactivity. These results highlight the need for advanced combustion models that can capture local differential diffusion and demixing effects—an essential requirement for accurately simulating hydrogen-enriched fuels in next-generation clean energy systems.

CRediT authorship contribution statement

Hendrik Nicolai: Writing – original draft, Visualization, Supervision, Software, Methodology, Investigation, Formal analysis, Data curation, Conceptualization. **Vinzenz Schuh:** Writing – review & editing, Methodology, Investigation, Data curation. **Antonia Bähr:** Writing – review & editing, Visualization, Investigation, Data curation. **Max Schneider:** Writing – review & editing, Visualization, Software, Methodology, Data curation. **Felix Rong:** Writing – review & editing, Visualization, Formal analysis, Data curation. **Driss Kaddar:** Writing – review & editing, Software, Data curation. **Mathis Bode:** Writing – review & editing, Software, Project administration. **Christian Hasse:** Writing – review & editing, Resources, Project administration, Funding acquisition.

Declaration of competing interest

The authors declare that they have no known competing financial interests or personal relationships that could have appeared to influence the work reported in this paper.

Acknowledgments

This research has been funded by the German Federal Ministry for Economics and Climate Action under the Federal Aeronautical Research Program under grant 20M2237E (LuFo VI, Call 2). The research leading to these results has received funding from EuroHPC within the Inno4Scale project under Grant Agreement No 101118139.

The authors gratefully acknowledge the Gauss Centre for Supercomputing e.V. (www.gauss-centre.eu) for funding this project by providing computing time on the GCS Supercomputer JUWELS and via the JUPITER Research and Early Access Program (JUREAP) at Jülich Supercomputing Centre (JSC).

Appendix A. Supplementary data

Supplementary material related to this article can be found online at https://doi.org/10.1016/j.proci.2025.105885.

References

[1] H. Pitsch, The transition to sustainable combustion: Hydrogen-and carbon-based future fuels and methods for dealing with their challenges, Proc. Combust. Inst. 40 (1–4) (2024) 105638.
[2] G. Sivashinsky, Diffusional-thermal theory of cellular flames, Combust. Sci. Technol. 15 (3–4) (1977) 137–145.
[3] M. Matalon, C. Cui, J. Bechtold, Hydrodynamic theory of premixed flames: effects of stoichiometry, variable transport coefficients and arbitrary reaction orders, J. Fluid Mech. 487 (2003) 179–210.
[4] H. Böttler, D. Kaddar, T.J.P. Karpowski, F. Ferraro, A. Scholtissek, H. Nicolai, C. Hasse, Can flamelet manifolds capture the interactions of thermo-diffusive instabilities and turbulence in lean hydrogen flames?—an a-priori analysis, Int. J. Hydrog. Energ. 56 (2024) 1397–1407.
[5] A. Aspden, M. Day, J. Bell, Turbulence–flame interactions in lean premixed hydrogen: transition to the distributed burning regime, J. Fluid Mech. 680 (2011) 287–320.
[6] A.N. Lipatnikov, H. Lee, P. Dai, M. Wan, V.A. Sabelnikov, Transition from turbulence-dominated to instability-dominated combustion regime in lean hydrogen-air flames, Combust. Flame 259 (2024) 113170.
[7] M. Rieth, A. Gruber, F.A. Williams, J.H. Chen, Enhanced burning rates in hydrogen-enriched turbulent premixed flames by diffusion of molecular and atomic hydrogen, Combust. Flame 239 (2022) 111740.

[8] L. Berger, A. Attili, H. Pitsch, Synergistic interactions of thermodiffusive instabilities and turbulence in lean hydrogen flames, Combust. Flame 244 (2022) 112254.
[9] L. Berger, A. Attili, M. Gauding, H. Pitsch, Effects of karlovitz number variations on thermodiffusive instabilities in lean turbulent hydrogen jet flames, Proc. Combust. Inst. 40 (1–4) (2024) 105219.
[10] J. Gaucherand, D. Laera, C. Schulze-Netzer, T. Poinsot, Dns of turbulent premixed ammonia/hydrogen flames: The impact of thermo-diffusive effects, Flow. Turbul. Combust. 112 (2) (2024) 587–614.
[11] C. Netzer, A. Ahmed, A. Gruber, T. Løvås, Curvature effects on no formation in wrinkled laminar ammonia/hydrogen/nitrogen-air premixed flames, Combust. Flame 232 (2021) 111520.
[12] S. Wiseman, M. Rieth, A. Gruber, J.R. Dawson, J.H. Chen, A comparison of the blow-out behavior of turbulent premixed ammonia/hydrogen/nitrogen-air and methane–air flames, Proc. Combust. Inst. 38 (2) (2021) 2869–2876.
[13] M. Rieth, A. Gruber, J.H. Chen, A direct numerical simulation study on NO and N2O formation in turbulent premixed ammonia/hydrogen/nitrogen-air flames, Proc. Combust. Inst. 39 (2) (2023) 2279–2288.
[14] G. Yu, C. Law, C. Wu, Laminar flame speeds of hydrocarbon+ air mixtures with hydrogen addition, Combust. Flame 63 (3) (1986) 339–347.
[15] F. Halter, C. Chauveau, N. Djebaïli-Chaumeix, I. Gökalp, Characterization of the effects of pressure and hydrogen concentration on laminar burning velocities of methane–hydrogen–air mixtures, Proc. Combust. Inst. 30 (1) (2005) 201–208.
[16] E.C. Okafor, A. Hayakawa, Y. Nagano, T. Kitagawa, Effects of hydrogen concentration on premixed laminar flames of hydrogen–methane–air, Int. J. Hydrog. Energy 39 (5) (2014) 2409–2417.
[17] M. Reyes, R. Sastre, F. Tinaut, J. Rodríguez-Fernández, Study and characterization of the instabilities generated in expanding spherical flames of hydrogen/methane/air mixtures, Int. J. Hydrog. Energ. 47 (53) (2022) 22616–22632.
[18] H. Lulic, A. Breicher, A. Scholtissek, P.E. Lapenna, A. Dreizler, F. Creta, C. Hasse, D. Geyer, F. Ferraro, On polyhedral structures of lean methane/hydrogen bunsen flames: combined experimental and numerical analysis, Proc. Combust. Inst. 39 (2) (2023) 1977–1986.
[19] F.H. Vance, H. Nicolai, C. Hasse, A numerical investigation into the stabilization of hydrogen enriched n-dodecane premixed flames, Int. J. Hydrog. Energ. 56 (2024) 611–620.
[20] H. Nicolai, L. Dressler, J. Janicka, C. Hasse, Assessing the importance of differential diffusion in stratified hydrogen–methane flames using extended flamelet tabulation approaches, Phys. Fluids 34 (8) (2022).
[21] V. Schuh, D. Kaddar, A. Bähr, M. Bode, C. Hasse, H. Nicolai, An extended artificially thickened flame model for turbulent hydrogen and hydrogen-enriched flames with intrinsic instabilities under gas turbine relevant conditions, J. Eng. Gas Turbines Power (2025).
[22] E.R. Hawkes, J.H. Chen, Direct numerical simulation of hydrogen-enriched lean premixed methane–air flames, Combust. Flame 138 (3) (2004) 242–258.
[23] T. Howarth, M.S. Day, H. Pitsch, A. Aspden, Thermal diffusion exhaust gas recirculation and blending effects on lean premixed hydrogen flames, Proc. Combust. Inst. 40 (1–4) (2024) 105429.
[24] V. Schuh, C. Hasse, H. Nicolai, An extension of the artificially thickened flame approach for premixed hydrogen flames with intrinsic instabilities, Proc. Combust. Inst. 40 (1–4) (2024) 105673.
[25] L. Esclapez, M. Day, J. Bell, A. Felden, C. Gilet, R. Grout, M.H. de Frahan, E. Motheau, A. Nonaka, L. Owen, et al., Pelelmex: an amr low mach number reactive flow simulation code without level sub-cycling, J. Open Source Softw. 8 (2023) (NREL/JA-2C00-85410).
[26] S. Kerkemeier, C.E. Frouzakis, A.G. Tomboulides, P. Fischer, M. Bode, nekCRF: A next generation high-order reactive low Mach flow solver for direct numerical simulations, 2024.
[27] A. Tomboulides, J. Lee, S. Orszag, Numerical simulation of low mach number reactive flows, J. Sci. Comput. 12 (1997) 139–167.
[28] R.J. Kee, M.E. Coltrin, P. Glarborg, H. Zhu, Chemically Reacting Flow: Theory, Modeling, and Simulation, John Wiley & Sons, 2017.
[29] M.D. Smooke, V. Giovangigli, Formulation of the premixed and nonpremixed test problems, Reduc. Kinet. Mech. Asymptot. Approx. Methane-Air Flames 384 (1991) 1–28.
[30] P. Fischer, S. Kerkemeier, M. Min, Y.-H. Lan, M. Phillips, T. Rathnayake, E. Merzari, A. Tomboulides, A. Karakus, N. Chalmers, T. Warburton, NekRS a GPU-accelerated spectral element Navier–Stokes solver, Parallel Comput. 114 (2022) 102982.
[31] T. Howarth, A. Aspden, An empirical characteristic scaling model for freely-propagating lean premixed hydrogen flames, Combust. Flame 237 (2022) 111805.
[32] D.G. Goodwin, R.L. Speth, H.K. Moffat, B.W. Weber, Cantera: An Object-Oriented Software Toolkit for Chemical Kinetics, Thermodynamics, and Transport Processes, Zenodo, 2018.